

Point integral method for elliptic equations with variable coefficients on point cloud[†]

Zhen Li¹, Zuqiang Shi^{2,*}, Jian Sun³

¹ Yau Mathematical Sciences Center, Tsinghua University, Beijing, China, 100084

² Department of Mathematical Sciences & Yau Mathematical Sciences Center, Tsinghua University, Beijing, China, 100084

³ Yau Mathematical Sciences Center, Tsinghua University, Beijing, China, 100084

Abstract. In this paper, we generalize the point integral method proposed in [25,39] to solve the general elliptic PDEs with variable coefficients and corresponding eigenvalue problems with Neumann, Robin and Dirichlet boundary conditions on point cloud. The main idea is using integral equations to approximate the original PDEs. The integral equations are easy to discretize on the point cloud. The truncation error of the integral approximation is analyzed. Numerical examples are presented to demonstrate that PIM is an effective method to solve the elliptic PDEs with smooth coefficients on point cloud.

Keywords: point integral method, elliptic equation, variable coefficients, point clouds.

1 Introduction

In the past decades, data play more and more important role in sciences and engineering, even in our daily life. Among varieties of models in data analysis, manifold based model attracts more and more attentions [3,6–9,16,18,20,21,27–29,31,32,34–36,40]. In the manifold model, data or images are associated to a smooth manifold embedded in a high dimensional Euclidean space. PDEs on the manifold, particularly the Laplace-Beltrami equation, give us powerful tools to reveal the underlying structure of the manifold. Usually, in data analysis and image processing, the manifold is represented as a collection of unstructured points in high dimensional space, which is referred as point cloud. To solve PDEs in point cloud, the traditional methods for PDEs on Euclidean space may not work.

Among varieties of manifolds, 2D surfaces embedded in \mathbb{R}^3 play very important role in many scientific and engineering problems, including material science [5,13], fluid flow

[†]Research supported by NSFC Grant 11371220, 11671005.

*Corresponding author. Email address: lishen03@gmail.com (Z. Li), zqshi@tsinghua.edu.cn (Z. Shi), jsun@math.tsinghua.edu.cn (J. Sun)

[15, 17], biology and biophysics [1, 2, 14, 33]. Many numerical methods to solve surface PDEs have been developed in the past decades, such as surface finite element method [12], level set method [4, 41], grid based particle method [22, 23] and closest point method [30, 37]. Finite element method has very good theoretical properties. It is shown that FEM converges quadratically in L^2 norm and linearly in H^1 norm for solving the Poisson equations [11]. However, to apply FEM, global mesh is needed which is not easy to generate especially in high dimensional space. The other methods, including level set method, grid based particle method, closest point method, also need extra information. These information is not easy to obtain from point cloud, especially in high dimensional space.

Due to the development of data and imaging science, solving PDEs on high dimensional unstructured point cloud absorb more and more attentions. Many researchers from different areas are trying to find alternative methods to discretize differential operators on high dimensional point cloud. Liang et al. proposed a method based on local least square approximations of the manifold [26]. Later, Lai et al. proposed the local mesh method to approximate differential operators on point cloud [19]. Despite of lack of proof, moving least square and local mesh based methods achieve high order accuracy and have achieved great successes in many applications.

The other numerical method in point cloud for Poisson equation is the point integral method (PIM) [25, 39]. The main idea of the point integral method is to approximate the Poisson equation via an integral equation:

$$\begin{aligned} -\int_{\mathcal{M}} \Delta_{\mathcal{M}} u(\mathbf{y}) \bar{R}_t(\mathbf{x}, \mathbf{y}) d\mathbf{y} &\approx \frac{1}{t} \int_{\mathcal{M}} R_t(\mathbf{x}, \mathbf{y}) (u(\mathbf{x}) - u(\mathbf{y})) d\mathbf{y} \\ &\quad - 2 \int_{\partial\mathcal{M}} \bar{R}_t(\mathbf{x}, \mathbf{y}) \frac{\partial u}{\partial \mathbf{n}}(\mathbf{y}) d\tau_y, \end{aligned} \quad (1.1)$$

where \mathbf{n} is the out normal of $\partial\mathcal{M}$, \mathcal{M} is a smooth d -dimensional manifold embedded in \mathbb{R}^N , $\partial\mathcal{M}$ is the boundary of \mathcal{M} . $R_t(\mathbf{x}, \mathbf{y})$ and $\bar{R}_t(\mathbf{x}, \mathbf{y})$ are kernel functions given as follows

$$R_t(\mathbf{x}, \mathbf{y}) = C_t R\left(\frac{|\mathbf{x}-\mathbf{y}|^2}{4t}\right), \quad \bar{R}_t(\mathbf{x}, \mathbf{y}) = C_t \bar{R}\left(\frac{|\mathbf{x}-\mathbf{y}|^2}{4t}\right)$$

where $C_t = \frac{1}{(4\pi t)^{d/2}}$ is the normalizing factor. $R \in C^2(\mathbb{R}^+)$ be a positive function that is integrable over $[0, +\infty)$,

$$\bar{R}(r) = \int_r^{+\infty} R(s) ds. \quad (1.2)$$

$\Delta_{\mathcal{M}}$ is the Laplace-Beltrami operator (LBO) on \mathcal{M} . The integral equation is much easier to discretize on point clouds with proper quadrature rule.

In this paper, we generalize PIM to solve general elliptic equations on manifold \mathcal{M} . We assume that $\mathcal{M} \in C^2$ is a compact d -dimensional manifold isometrically embedded in \mathbb{R}^N with the standard Euclidean metric and $d \leq N$. If \mathcal{M} has boundary, the boundary, $\partial\mathcal{M}$ is also a C^2 smooth manifold.

Let $X: V \subset \mathbb{R}^d \rightarrow \mathcal{M} \subset \mathbb{R}^N$ be a local parametrization of \mathcal{M} and $\theta \in V$. For any differentiable function $f: \mathcal{M} \rightarrow \mathbb{R}$, let $F(\theta) = f(X(\theta))$, define

$$D_k f(X(\theta)) = \sum_{i,j=1}^m g^{ij}(\theta) \frac{\partial X_k}{\partial \theta_i}(\theta) \frac{\partial F}{\partial \theta_j}(\theta), \quad k=1, \dots, N. \quad (1.3)$$

where $(g^{ij})_{i,j=1,\dots,d} = G^{-1}$ and $G(\theta) = (g_{ij})_{i,j=1,\dots,d}$ is the first fundamental form which is defined by

$$g_{ij}(\theta) = \sum_{k=1}^N \frac{\partial X_k}{\partial \theta_i}(\theta) \frac{\partial X_k}{\partial \theta_j}(\theta), \quad i,j=1, \dots, d. \quad (1.4)$$

The general second order elliptic PDE on manifold \mathcal{M} has following form,

$$-\sum_{i,j=1}^N D_i(a^{ij}(\mathbf{x}) D_j u(\mathbf{x})) + \sum_{j=1}^N b^j(\mathbf{x}) D_j u(\mathbf{x}) + c(\mathbf{x}) u(\mathbf{x}) = f(\mathbf{x}), \quad \mathbf{x} \in \mathcal{M} \quad (1.5)$$

The coefficients $a^{ij}(\mathbf{x})$, $b^j(\mathbf{x})$, $c(\mathbf{x})$ and source term $f(\mathbf{x})$ are known smooth functions of spatial variables, i.e.

$$a^{ij}, b^j, c, f \in C^1(\mathcal{M}), \quad i,j=1, \dots, N.$$

The matrix $A(\mathbf{x}) = (a^{ij})_{i,j=1,\dots,N}$ is symmetric and maps the tangent space $T_{\mathbf{x}}\mathcal{M}$ into itself and satisfies following elliptic condition: there exist generic constants $0 < a_0, a_1 < \infty$ independent on \mathbf{x} such that for any $\xi = [\xi_1, \dots, \xi_N]^t \in \mathbb{R}^N$,

$$a_0 \sum_{i=1}^N \xi_i^2 \leq \sum_{i,j=1}^N a^{ij}(\mathbf{x}) \xi_i \xi_j \leq a_1 \sum_{i=1}^N \xi_i^2 \quad (1.6)$$

The main contribution of this paper is to generalize the point integral method to solve the general elliptic equation (1.5). The essential ingredient in PIM is the integral approximation of the differential operators. To approximate the elliptic equations (1.5), we need two integral approximations for second order and first order term.

To approximate the second order term, we need to incorporate the coefficients, a^{ij} , in the kernel functions. More precisely, we use kernel functions as follows:

$$R_t(\mathbf{x}, \mathbf{y}) = C_t R \left(\frac{1}{4t} \sum_{i,j=1}^N a_{ij}(\mathbf{x}) (x_i - y_i)(x_j - y_j) \right), \quad (1.7)$$

$$\bar{R}_t(\mathbf{x}, \mathbf{y}) = C_t \bar{R} \left(\frac{1}{4t} \sum_{i,j=1}^N a_{ij}(\mathbf{x}) (x_i - y_i)(x_j - y_j) \right) \quad (1.8)$$

where \bar{R} and R satisfy the relation in (1.2),

$$(a_{ij}(\mathbf{x}))_{i,j=1,\dots,N} = (A(\mathbf{x}))^{-1}, \quad A(\mathbf{x}) = (a^{ij}(\mathbf{x}))_{i,j=1,\dots,N}.$$

With above kernel functions, we can prove following integral approximation for second order term in (1.5).

$$\begin{aligned} -\int_{\mathcal{M}} \sum_{i,j=1}^N a^{ij}(\mathbf{y}) D_{ij} u(\mathbf{y}) \bar{R}_t(\mathbf{x}, \mathbf{y}) d\mathbf{y} &\approx \frac{1}{t} \int_{\mathcal{M}} (u(\mathbf{x}) - u(\mathbf{y})) R_t(\mathbf{x}, \mathbf{y}) d\mathbf{y} \\ &\quad - 2 \int_{\partial\mathcal{M}} \sum_{i,j=1}^N n_i(\mathbf{y}) a^{ij}(\mathbf{y}) D_j u(\mathbf{y}) \bar{R}_t(\mathbf{x}, \mathbf{y}) d\tau_{\mathbf{y}}. \end{aligned} \quad (1.9)$$

Using the same kernel function, the integral approximation of the first order term is

$$\begin{aligned} \int_{\mathcal{M}} \sum_{j=1}^N b^j(\mathbf{y}) D_j u(\mathbf{y}) \bar{R}_t(\mathbf{x}, \mathbf{y}) d\mathbf{y} &\approx \\ \frac{1}{2t} \int_{\mathcal{M}} \sum_{j,k=1}^N b^j(\mathbf{y}) a_{jk}(\mathbf{x}) (x^k - y^k) (u(\mathbf{x}) - u(\mathbf{y})) R_t(\mathbf{x}, \mathbf{y}) d\mathbf{y}. \end{aligned} \quad (1.10)$$

Using these two integral approximations, the elliptic equation (1.5) is approximated by an integral equation. On the point cloud, the integral equation is much easier to discretize. Therefore, a discretization of the elliptic equation (1.5) on point cloud is derived.

The rest of the paper is organized as follows. In Section 2, we derive the integral approximations, (1.9) and (1.10). Errors of the approximations are analyzed. Based on the integral approximations, point integral method for the elliptic equation (1.5) is given in Section 3. Section 4 is devoted to numerical examples. In the end, conclusions are made in Section 5.

2 Integral Approximation

In this section, we analyze the error in the integral approximations, (1.9) and (1.10). In previous papers [24, 39], we proved the convergence of the point integral method for elliptic equations with isotropic coefficients. With anisotropic coefficients, the integral approximations proposed in this paper do not preserve the symmetry of the original elliptic operator, which makes the convergence difficult to analyze. So only local truncation error is obtained. To get the local truncation error, some assumptions are listed in Assumption 1.

Assumption 1.

1. Smoothness of the manifold: $\mathcal{M}, \partial\mathcal{M}$ are both compact and C^∞ smooth d -dimensional submanifolds isometrically embedded in a Euclidean space \mathbb{R}^N .

2. Smoothness of the coefficients: $a^{ij} \in C^2(\mathcal{M})$.

3. Assumptions on the kernel function $R(r)$:

(a) Boundness: $R(r)$ is bounded;

(b) Compact support: $R(r) = 0$ for $\forall r > 1$;

All the analysis in this section is carried out under above assumptions. In the statements of the theorems in this section, we omit above assumptions to make the theorems more concise. Regarding the integral approximation of the second order term (1.9), we have theorem as follows.

Theorem 2.1. *For any $u \in C^3(\mathcal{M})$, let*

$$\begin{aligned} R_{II}(\mathbf{x}) = & \int_{\mathcal{M}} \sum_{i,j=1}^N a^{ij}(\mathbf{y}) D_{ij} u(\mathbf{y}) \bar{R}_t(\mathbf{x}, \mathbf{y}) d\mathbf{y} + \frac{1}{t} \int_{\mathcal{M}} (u(\mathbf{x}) - u(\mathbf{y})) R_t(\mathbf{x}, \mathbf{y}) d\mathbf{y} \\ & - 2 \int_{\partial\mathcal{M}} \sum_{i,j=1}^N n_i(\mathbf{y}) a^{ij}(\mathbf{y}) D_j u(\mathbf{y}) \bar{R}_t(\mathbf{x}, \mathbf{y}) d\tau_y. \end{aligned}$$

where $\mathbf{n} = (n_1, \dots, n_d)$ is the out normal of $\partial\mathcal{M}$, $R_t(\mathbf{x}, \mathbf{y})$ and $\bar{R}_t(\mathbf{x}, \mathbf{y})$ are kernel functions given in (1.7) and (1.8) and $D_{ij} = D_i(D_j)$ is the second order derivative operator.

There exists constants C, T_0 depending only on $\mathcal{M}, \partial\mathcal{M}$, so that for any $t \leq T_0$,

$$\|R_{II} - I_{bd}\|_{L^2(\mathcal{M})} = Ct^{1/2} \|u\|_{C^3(\mathcal{M})}. \quad (2.1)$$

with

$$\begin{aligned} I_{bd} = & \int_{\partial\mathcal{M}} \sum_{i,m,n=1}^N n_i(\mathbf{y}) a_{im}(\mathbf{x}) \bar{R}_t(\mathbf{x}, \mathbf{y}) D_m D_n u(\mathbf{y}) (x_n - y_n) d\tau_y \\ & - 2 \int_{\partial\mathcal{M}} \sum_{i,j=1}^N n_i(\mathbf{y}) (a_{ij}(\mathbf{y}) - a_{ij}(\mathbf{x})) \bar{R}_t(\mathbf{x}, \mathbf{y}) D_j u(\mathbf{y}) d\tau_y. \end{aligned}$$

Moreover,

$$\|I_{bd}\|_{L^2(\mathcal{M})} = O(t^{1/4}).$$

Proof. In the proof, we use Einstein's convention for repeated indices.

First of all, integration by parts gives that

$$\begin{aligned} & \int_{\mathcal{M}} D_i (a_{ij}(\mathbf{y}) D_j u(\mathbf{y})) \bar{R}_t(\mathbf{x}, \mathbf{y}) d\mathbf{y} \\ & = - \int_{\mathcal{M}} a_{ij}(\mathbf{y}) D_j u(\mathbf{y}) D_i \bar{R}_t(\mathbf{x}, \mathbf{y}) d\mathbf{y} + \int_{\partial\mathcal{M}} n_i(\mathbf{y}) a_{ij}(\mathbf{y}) D_j u(\mathbf{y}) \bar{R}_t(\mathbf{x}, \mathbf{y}) d\tau_y \end{aligned} \quad (2.2)$$

Substituting above expansion in the first term of (2.2), we get

$$\begin{aligned} & - \int_{\mathcal{M}} a_{ij}(\mathbf{y}) D_j u(\mathbf{y}) D_i \bar{R}_t(\mathbf{x}, \mathbf{y}) d\mathbf{y} \\ = & - \frac{1}{2t} \int_{\mathcal{M}} a_{ij}(\mathbf{y}) (\partial_{l'} \Phi^j g^{l'k'} \partial_j u(\mathbf{y})) \partial_{i'} \Phi^i g^{i'j'} \partial_{j'} \Phi^n a^{mn}(\mathbf{x}) (x_m - y_m) R_t(\mathbf{x}, \mathbf{y}) d\mathbf{y} \end{aligned} \quad (2.3)$$

The coefficients $a_{ij}(\mathbf{y})$ maps the tangent space $T_y \mathcal{M}$ into itself which means that there exists $c_{l'l}(\mathbf{y})$ such that

$$a_{ij}(\mathbf{y}) \partial_{l'} \Phi^j = c_{l'l}(\mathbf{y}) \partial_l \Phi^i.$$

Then

$$\begin{aligned} & - \int_{\mathcal{M}} a_{ij}(\mathbf{y}) D_j u(\mathbf{y}) D_i \bar{R}_t(\mathbf{x}, \mathbf{y}) d\mathbf{y} \\ = & - \frac{1}{2t} \int_{\mathcal{M}} c_{l'l}(\mathbf{y}) \partial_l \Phi^i \partial_{i'} \Phi^i g^{l'k'} g^{i'j'} \partial_{j'} \Phi^n a^{mn}(\mathbf{x}) (x_m - y_m) R_t(\mathbf{x}, \mathbf{y}) \partial_{k'} u(\mathbf{y}) d\mathbf{y} \\ = & - \frac{1}{2t} \int_{\mathcal{M}} c_{l'j'}(\mathbf{y}) \partial_{j'} \Phi^n g^{l'k'} a^{mn}(\mathbf{x}) (x_m - y_m) R_t(\mathbf{x}, \mathbf{y}) \partial_{k'} u(\mathbf{y}) d\mathbf{y} \\ = & - \frac{1}{2t} \int_{\mathcal{M}} a_{nl}(\mathbf{y}) \partial_{l'} \Phi^l g^{l'k'} a^{mn}(\mathbf{x}) (x_m - y_m) R_t(\mathbf{x}, \mathbf{y}) \partial_{k'} u(\mathbf{y}) d\mathbf{y} \\ = & - \frac{1}{2t} \int_{\mathcal{M}} a_{nl}(\mathbf{y}) a^{mn}(\mathbf{x}) (x_m - y_m) R_t(\mathbf{x}, \mathbf{y}) D_l u(\mathbf{y}) d\mathbf{y} \\ = & - \frac{1}{2t} \int_{\mathcal{M}} (a_{nl}(\mathbf{y}) - a_{nl}(\mathbf{x})) a^{mn}(\mathbf{x}) (x_m - y_m) R_t(\mathbf{x}, \mathbf{y}) D_l u(\mathbf{y}) d\mathbf{y} \\ & - \frac{1}{2t} \int_{\mathcal{M}} (x_l - y_l) D_l u(\mathbf{y}) R_t(\mathbf{x}, \mathbf{y}) d\mathbf{y}. \end{aligned} \quad (2.4)$$

Notice that

$$\begin{aligned} D_n \bar{R}_t(\mathbf{x}, \mathbf{y}) &= \frac{1}{2t} \partial_{i'} \Phi^n g^{i'j'} \partial_{j'} \Phi^l a^{ml}(\mathbf{x}) (x_m - y_m) R_t(\mathbf{x}, \mathbf{y}) \\ &= \frac{1}{2t} \partial_{i'} \Phi^n g^{i'j'} \partial_{j'} \Phi^l a^{ml}(\mathbf{y}) \partial_{m'} \Phi^m (\alpha_{m'} - \beta_{m'}) R_t(\mathbf{x}, \mathbf{y}) + O(1) \end{aligned} \quad (2.5)$$

Since $a^{ml}(\mathbf{y})$ also maps the tangent space $T_y \mathcal{M}$ into itself, there exists $d_{l'l}(\mathbf{y})$ such that

$$a^{ml}(\mathbf{y}) \partial_{m'} \Phi^m = d_{m'l'}(\mathbf{y}) \partial_{l'} \Phi^l.$$

It follows that

$$\begin{aligned}
D_n \bar{R}_t(\mathbf{x}, \mathbf{y}) &= \frac{1}{2t} d_{m'l'}(\mathbf{y}) \partial_{l'} \Phi^l \partial_{j'} \Phi^l g^{i'j'} \partial_{i'} \Phi^n (\alpha_{m'} - \beta_{m'}) R_t(\mathbf{x}, \mathbf{y}) + O(1) \\
&= \frac{1}{2t} d_{m'i'}(\mathbf{y}) \partial_{i'} \Phi^n (\alpha_{m'} - \beta_{m'}) R_t(\mathbf{x}, \mathbf{y}) + O(1) \\
&= \frac{1}{2t} a^{mn}(\mathbf{y}) \partial_{m'} \Phi^m (\alpha_{m'} - \beta_{m'}) R_t(\mathbf{x}, \mathbf{y}) + O(1) \\
&= \frac{1}{2t} a^{mn}(\mathbf{y}) (x_m - y_m) R_t(\mathbf{x}, \mathbf{y}) + O(1) \\
&= \frac{1}{2t} a^{mn}(\mathbf{x}) (x_m - y_m) R_t(\mathbf{x}, \mathbf{y}) + O(1)
\end{aligned} \tag{2.6}$$

The last term of (2.4) becomes

$$\begin{aligned}
&\frac{1}{2t} \int_{\mathcal{M}} (a_{nl}(\mathbf{y}) - a_{nl}(\mathbf{x})) a^{mn}(\mathbf{x}) (x_m - y_m) R_t(\mathbf{x}, \mathbf{y}) D_l u(\mathbf{y}) d\mathbf{y} \\
&= \int_{\mathcal{M}} (a_{nl}(\mathbf{y}) - a_{nl}(\mathbf{x})) D_n^y \bar{R}_t(\mathbf{x}, \mathbf{y}) D_l u(\mathbf{y}) d\mathbf{y} + O(\sqrt{t}) \\
&= - \int_{\mathcal{M}} D_n a_{nl}(\mathbf{y}) D_l u(\mathbf{y}) \bar{R}_t(\mathbf{x}, \mathbf{y}) d\mathbf{y} \\
&\quad + \int_{\partial \mathcal{M}} n_n(\mathbf{y}) (a_{nl}(\mathbf{y}) - a_{nl}(\mathbf{x})) \bar{R}_t(\mathbf{x}, \mathbf{y}) D_l u(\mathbf{y}) d\tau_{\mathbf{y}} + O(\sqrt{t})
\end{aligned} \tag{2.7}$$

Now, we turn to estimate the first term of (2.4). In this step, we need the help of Taylor's expansion of $u(\mathbf{x})$ at \mathbf{y} ,

$$u(\mathbf{x}) - u(\mathbf{y}) = (x_j - y_j) D_j u(\mathbf{y}) + \frac{1}{2} D_m D_n u(\mathbf{y}) (x_m - y_m) (x_n - y_n) + O(\|\mathbf{x} - \mathbf{y}\|^3) \tag{2.8}$$

This expansion gives immediately

$$\begin{aligned}
&- \frac{1}{2t} \int_{\mathcal{M}} (x_j - y_j) D_j u(\mathbf{y}) R_t(\mathbf{x}, \mathbf{y}) d\mathbf{y} \\
&= - \frac{1}{2t} \int_{\mathcal{M}} R_t(\mathbf{x}, \mathbf{y}) (u(\mathbf{x}) - u(\mathbf{y})) d\mathbf{y} \\
&\quad + \frac{1}{4t} \int_{\mathcal{M}} R_t(\mathbf{x}, \mathbf{y}) D_m D_n u(\mathbf{y}) (x_m - y_m) (x_n - y_n) d\mathbf{y} + O(\sqrt{t}).
\end{aligned} \tag{2.9}$$

Next, we focus on the second term of (2.9). It follows from (2.6) that

$$\begin{aligned}
a_{im}(\mathbf{x}) D_i \bar{R}_t(\mathbf{x}, \mathbf{y}) &= \frac{1}{2t} a_{mi}(\mathbf{x}) a^{m'i}(\mathbf{x}) (x_{m'} - y_{m'}) R_t(\mathbf{x}, \mathbf{y}) + O(1) \\
&= \frac{1}{2t} a_{mi}(\mathbf{x}) a^{m'i}(\mathbf{x}) (x_{m'} - y_{m'}) R_t(\mathbf{x}, \mathbf{y}) + O(1) \\
&= \frac{1}{2t} (x_m - y_m) R_t(\mathbf{x}, \mathbf{y}) + O(1)
\end{aligned} \tag{2.10}$$

The second term of (2.9) is calculated as

$$\begin{aligned}
& \frac{1}{4t} \int_{\mathcal{M}} R_t(\mathbf{x}, \mathbf{y}) D_m D_n u(\mathbf{y}) (x_m - y_m) (x_n - y_n) d\mathbf{y} \\
&= \frac{1}{2} \int_{\mathcal{M}} a_{im}(\mathbf{x}) D_i \bar{R}_t(\mathbf{x}, \mathbf{y}) D_m D_n u(\mathbf{y}) (x_n - y_n) d\mathbf{y} \\
&= \frac{1}{2} \int_{\mathcal{M}} a_{im}(\mathbf{x}) (\partial_{i'} \Phi^i g^{i'j'} \partial_{j'} \Phi^n) D_m D_n u(\mathbf{y}) \bar{R}_t(\mathbf{x}, \mathbf{y}) d\mathbf{y} \\
&\quad + \frac{1}{2} \int_{\partial\mathcal{M}} n_i(\mathbf{y}) a_{im}(\mathbf{x}) \bar{R}_t(\mathbf{x}, \mathbf{y}) D_m D_n u(\mathbf{y}) (x_n - y_n) d\mathbf{y}.
\end{aligned} \tag{2.11}$$

Notice that

$$\begin{aligned}
& a_{im}(\mathbf{x}) (\partial_{i'} \Phi^i g^{i'j'} \partial_{j'} \Phi^n) D_m \\
&= a_{im}(\mathbf{y}) (\partial_{i'} \Phi^i g^{i'j'} \partial_{j'} \Phi^n) (\partial_{i''} \Phi^m g^{i''j''} \partial_{j''}) + O(\sqrt{t}) \\
&= c_{i''l} \partial_l \Phi^i \partial_{i'} \Phi^i g^{i'j'} \partial_{j'} \Phi^n g^{i''j''} \partial_{j''} + O(\sqrt{t}) \\
&= c_{i''l} \partial_l \Phi^n g^{i''j''} \partial_{j''} + O(\sqrt{t}) \\
&= a_{mn} \partial_{i''} \Phi^m g^{i''j''} \partial_{j''} + O(\sqrt{t}) \\
&= a_{mn} D_m + O(\sqrt{t})
\end{aligned}$$

From (2.11), we obtain

$$\begin{aligned}
& \frac{1}{4t} \int_{\mathcal{M}} R_t(\mathbf{x}, \mathbf{y}) D_m D_n u(\mathbf{y}) (x_m - y_m) (x_n - y_n) d\mathbf{y} \\
&= \frac{1}{2} \int_{\mathcal{M}} a_{mn}(\mathbf{x}) D_m D_n u(\mathbf{y}) \bar{R}_t(\mathbf{x}, \mathbf{y}) d\mathbf{y} \\
&\quad + \frac{1}{2} \int_{\partial\mathcal{M}} n_i(\mathbf{y}) a_{im}(\mathbf{x}) \bar{R}_t(\mathbf{x}, \mathbf{y}) D_m D_n u(\mathbf{y}) (x_n - y_n) d\mathbf{y} + O(\sqrt{t}).
\end{aligned} \tag{2.12}$$

Now, using (2.2), (2.4), (2.9) and (2.12), we get

$$\begin{aligned}
& \int_{\mathcal{M}} D_i (a_{ij}(\mathbf{y}) D_j u(\mathbf{y})) \bar{R}_t(\mathbf{x}, \mathbf{y}) d\mathbf{y} \\
&= -\frac{1}{2t} \int_{\mathcal{M}} R_t(\mathbf{x}, \mathbf{y}) (u(\mathbf{x}) - u(\mathbf{y})) d\mathbf{y} + \frac{1}{2} \int_{\mathcal{M}} a_{ij}(\mathbf{x}) D_m D_n u(\mathbf{y}) \bar{R}_t(\mathbf{x}, \mathbf{y}) d\mathbf{y} \\
&\quad + \int_{\mathcal{M}} D_i a_{ij}(\mathbf{x}) D_j u(\mathbf{y}) \bar{R}_t(\mathbf{x}, \mathbf{y}) d\mathbf{y} + \int_{\partial\mathcal{M}} n_i(\mathbf{y}) a_{ij}(\mathbf{y}) D_j u(\mathbf{y}) \bar{R}_t(\mathbf{x}, \mathbf{y}) d\mathbf{y} \\
&\quad + B.T. + O(\sqrt{t})
\end{aligned} \tag{2.13}$$

where

$$\begin{aligned}
B.T. &= \frac{1}{2} \int_{\partial\mathcal{M}} n_i(\mathbf{y}) a_{im}(\mathbf{x}) \bar{R}_t(\mathbf{x}, \mathbf{y}) D_m D_n u(\mathbf{y}) (x_n - y_n) d\tau_y \\
&\quad - \int_{\partial\mathcal{M}} n_i(\mathbf{y}) (a_{ij}(\mathbf{y}) - a_{ij}(\mathbf{x})) \bar{R}_t(\mathbf{x}, \mathbf{y}) D_j u(\mathbf{y}) d\tau_y
\end{aligned} \tag{2.14}$$

(2.1) is a direct implication of (2.13) and (2.14).

The boundary term I_{bd} can be calculated by a simple scaling argument. Since R_t is normalized, which has a coefficient $O(t^{-d/2})$ and the integral on the boundary absorbs $t^{-(d-1)/2}$, $(x-y)$ or $(a_{ij}(\mathbf{y}) - a_{ij}(\mathbf{x}))$ takes another $t^{-1/2}$, so I_{bd} is $O(1)$ in L_∞ . Moreover, \bar{R}_t is compactly supported, so the boundary term is nonzero only in a narrow layer adjacent to the boundary and the width of the layer is $O(\sqrt{t})$. Based on this simple argument, we can see

$$\|I_{bd}\|_{L^2} = O(t^{1/4}).$$

□

Theorem 2.2. For any $u \in C^1(\mathcal{M})$ and $b^j \in C^1(\mathcal{M})$, let

$$\begin{aligned} R_I(\mathbf{x}) &= \int_{\mathcal{M}} \sum_{j=1}^N b^j(\mathbf{y}) D_j u(\mathbf{y}) \bar{R}_t(\mathbf{x}, \mathbf{y}) \, d\mathbf{y} \\ &\quad - \frac{1}{2t} \int_{\mathcal{M}} \sum_{j,k=1}^N b^j(\mathbf{y}) a_{jk}(\mathbf{x}) (x^k - y^k) (u(\mathbf{x}) - u(\mathbf{y})) R_t(\mathbf{x}, \mathbf{y}) \, d\mathbf{y}. \end{aligned}$$

Then

$$\|R_I - J_{bd}\|_{L^2(\mathcal{M})} = O(t^{1/2}).$$

with J_{bd} is the boundary term,

$$J_{bd}(\mathbf{x}) = \int_{\partial\mathcal{M}} \sum_{j=1}^N n_j(\mathbf{y}) b^j(\mathbf{y}) (u(\mathbf{y}) - u(\mathbf{x})) \bar{R}_t(\mathbf{x}, \mathbf{y}) \, d\tau_y,$$

where $\mathbf{n} = (n_1, \dots, n_d)$ is the out normal of $\partial\mathcal{M}$. Moreover,

$$\|J_{bd}\|_{L^2(\mathcal{M})} = O(t^{1/4}).$$

Proof. The proof is straightforward by integration by parts.

$$\begin{aligned}
& \int_{\mathcal{M}} \sum_{j=1}^N b^j(\mathbf{y}) D_j u(\mathbf{y}) \bar{R}_t(\mathbf{x}, \mathbf{y}) \, d\mathbf{y} \\
&= \int_{\mathcal{M}} \sum_{j=1}^N b^j(\mathbf{y}) D_j(u(\mathbf{y}) - u(\mathbf{x})) \bar{R}_t(\mathbf{x}, \mathbf{y}) \, d\mathbf{y} \\
&= - \int_{\mathcal{M}} \sum_{j=1}^N b^j(\mathbf{y}) (u(\mathbf{y}) - u(\mathbf{x})) D_j \bar{R}_t(\mathbf{x}, \mathbf{y}) \, d\mathbf{y} \\
&\quad + \int_{\partial\mathcal{M}} \sum_{j=1}^N n_j b^j(\mathbf{y}) (u(\mathbf{y}) - u(\mathbf{x})) \bar{R}_t(\mathbf{x}, \mathbf{y}) \, d\tau_{\mathbf{y}} \\
&\quad - \int_{\mathcal{M}} \sum_{j=1}^N D_j b^j(\mathbf{y}) (u(\mathbf{y}) - u(\mathbf{x})) \bar{R}_t(\mathbf{x}, \mathbf{y}) \, d\mathbf{y} \\
&= \frac{1}{2t} \int_{\mathcal{M}} \sum_{j,k=1}^N b^j(\mathbf{y}) a_{jk}(\mathbf{x}) (y^k - x^k) (u(\mathbf{y}) - u(\mathbf{x})) R_t(\mathbf{x}, \mathbf{y}) \, d\mathbf{y} + J_{bd}(\mathbf{x}) + O(\sqrt{t}),
\end{aligned}$$

where $\mathbf{n} = (n_1, \dots, n_d)$ is the out normal of $\partial\mathcal{M}$. \square

3 Point Integral Method

Now, we derive the point integral method for general second order elliptic equation (1.5) based on the integral approximations proved in the previous section. Consider the general second order elliptic equation

$$-\sum_{i,j=1}^N D_i(a^{ij}(\mathbf{x}) D_j u(\mathbf{x})) + \sum_{j=1}^N b^j(\mathbf{x}) D_j u(\mathbf{x}) + c(\mathbf{x}) u(\mathbf{x}) = f(\mathbf{x}), \quad \mathbf{x} \in \mathcal{M}.$$

Multiplying the kernel function $\bar{R}_t(\mathbf{x}, \mathbf{y})$ on both sides and using Theorems 2.1, 2.2, it is easy to get an integral equation to approximate the original elliptic equation:

$$L_t u(\mathbf{x}) - \int_{\partial\mathcal{M}} \bar{R}_t(\mathbf{x}, \mathbf{y}) \sum_{i,j=1}^N n_i(\mathbf{y}) a^{ij}(\mathbf{y}) D_j u(\mathbf{y}) \, d\tau_{\mathbf{y}} = \int_{\mathcal{M}} \bar{R}_t(\mathbf{x}, \mathbf{y}) f(\mathbf{y}) \, d\mathbf{y}, \quad (3.1)$$

where

$$L_t u(\mathbf{x}) = \frac{1}{t} \int_{\mathcal{M}} (u(\mathbf{x}) - u(\mathbf{y})) (1 - M(\mathbf{x}, \mathbf{y})) R_t(\mathbf{x}, \mathbf{y}) \, d\mathbf{y} + \int_{\mathcal{M}} c(\mathbf{y}) u(\mathbf{y}) \bar{R}_t(\mathbf{x}, \mathbf{y}) \, d\mathbf{y}, \quad (3.2)$$

and

$$M(\mathbf{x}, \mathbf{y}) = \frac{1}{2} \sum_{i,j,k=1}^N (b^j(\mathbf{y}) - D_i a^{ij}(\mathbf{y})) a_{jk}(\mathbf{x}) (y^k - x^k). \quad (3.3)$$

If both a^{ij} and $D_i a^{ij}$ are given, we can use the integral equation (3.1) directly. In many cases, only a^{ij} is given on the point cloud, we calculate $D_k a^{ij}$ based on the integral approximation in Theorem 2.2.

$$\int_{\mathcal{M}} D_k a^{ij}(\mathbf{y}) \bar{R}_t(\mathbf{x}, \mathbf{y}) d\mathbf{y} \approx \frac{1}{2t} \int_{\mathcal{M}} (a^{ij}(\mathbf{x}) - a^{ij}(\mathbf{y})) \sum_{l=1}^N a_{kl}(\mathbf{x})(x^l - y^l) R_t(\mathbf{x}, \mathbf{y}) d\mathbf{y},$$

Futhermore, under the assumption that $a^{ij} \in C^2(\mathcal{M})$, it is easy to get

$$\int_{\mathcal{M}} (D_k a^{ij}(\mathbf{x}) - D_k a^{ij}(\mathbf{y})) \bar{R}_t(\mathbf{x}, \mathbf{y}) d\mathbf{y} = O(\sqrt{t}).$$

Then, we have an approximation for $D_k a^{ij}(\mathbf{x})$

$$D_k a^{ij}(\mathbf{x}) = \frac{1}{2t} \int_{\mathcal{M}} (a^{ij}(\mathbf{x}) - a^{ij}(\mathbf{y})) \sum_{l=1}^N a_{kl}(\mathbf{x})(x^l - y^l) \hat{R}_t(\mathbf{x}, \mathbf{y}) d\mathbf{y} + R_4(\mathbf{x}),$$

where

$$\hat{R}_t(\mathbf{x}, \mathbf{y}) = R_t(\mathbf{x}, \mathbf{y}) / \int_{\mathcal{M}} \bar{R}_t(\mathbf{x}, \mathbf{y}) d\mathbf{y}.$$

The error of this approximation is $O(t^{1/4})$ in L^2 .

3.1 Boundary Conditions

Now, we consider to incoporate boundary conditions in the integral equation (3.1). The Neumann boundary condition is very easy to handle.

$$\sum_{i,j=1}^N n_i(\mathbf{x}) a^{ij}(\mathbf{x}) D_j u(\mathbf{x}) = g, \quad \mathbf{x} \in \partial \mathcal{M} \quad (3.4)$$

We only need to substitute above boundary condition in the integral equation directly,

$$L_t u(\mathbf{x}) - 2 \int_{\partial \mathcal{M}} \bar{R}_t(\mathbf{x}, \mathbf{y}) g(\mathbf{y}) d\tau_{\mathbf{y}} = \int_{\mathcal{M}} \bar{R}_t(\mathbf{x}, \mathbf{y}) f(\mathbf{y}) d\mathbf{y}, \quad (3.5)$$

The treatment of the Robin boundary condition is also natural in the integral equations.

$$u(\mathbf{x}) + \beta \sum_{i,j=1}^N n_i(\mathbf{x}) a^{ij}(\mathbf{x}) D_j u(\mathbf{x}) = g(\mathbf{x}), \quad \mathbf{x} \in \partial \mathcal{M} \quad (3.6)$$

It solves that

$$\sum_{i,j=1}^N n_i(\mathbf{x}) a^{ij}(\mathbf{x}) D_j u(\mathbf{x}) = \frac{1}{\beta} (g(\mathbf{x}) - u(\mathbf{x})).$$

Then the integral equation (3.1) becomes

$$L_t u(\mathbf{x}) - \frac{2}{\beta} \int_{\partial\mathcal{M}} (g(\mathbf{y}) - u(\mathbf{y})) \bar{R}_t(\mathbf{x}, \mathbf{y}) d\tau_y = \int_{\mathcal{M}} f(\mathbf{y}) \bar{R}_t(\mathbf{x}, \mathbf{y}) dy. \quad (3.7)$$

The Dirichlet boundary condition

$$u(\mathbf{x}) = g(\mathbf{x}), \quad \mathbf{x} \in \partial\mathcal{M} \quad (3.8)$$

is more difficult to deal with in PIM, since the normal derivative is not given. One simplest way is using Robin boundary condition to approximate the Dirichlet boundary condition,

$$u(\mathbf{x}) + \mu \sum_{i,j=1}^N n_i(\mathbf{x}) a^{ij}(\mathbf{x}) D_j u(\mathbf{x}) = g(\mathbf{x}), \quad \mathbf{x} \in \partial\mathcal{M} \quad (3.9)$$

with $\mu \ll 1$.

It is easy to show that solution of the Robin problem for equation (1.5) converges to that of the Dirichlet problem of the same equation, as $\mu \rightarrow 0$, see Appendix B.

An approximate solution of the Dirichlet problem is given by following integral equation with $\mu \ll 1$:

$$L_t u(\mathbf{x}) - \frac{2}{\mu} \int_{\partial\mathcal{M}} (g(\mathbf{y}) - u(\mathbf{y})) \bar{R}_t(\mathbf{x}, \mathbf{y}) d\tau_y = \int_{\mathcal{M}} f(\mathbf{y}) \bar{R}_t(\mathbf{x}, \mathbf{y}) dy. \quad (3.10)$$

This is the simplest way to enforce the Dirichlet boundary condition in the point integral method. We can also use Augmented Lagrange Multiplier (ALM) based method [25] or volume constraint [10, 38] to deal with the Dirichlet boundary condition.

3.2 Discretization

In the point integral method, the discretization is straightforward. The manifold is assumed to be sampled by a set of sample points P and a subset $S \subset P$ sampling the boundary of \mathcal{M} . List the points in P respectively S in a fixed order $P = (\mathbf{p}_1, \dots, \mathbf{p}_n)$ where $\mathbf{p}_i \in \mathbb{R}^N, 1 \leq i \leq n$, respectively $S = (\mathbf{s}_1, \dots, \mathbf{s}_{n_b})$ where $\mathbf{s}_i \in P$.

In addition, assume we are given two vectors $\mathbf{V} = (V_1, \dots, V_n)^t$ where V_i is an volume weight of \mathbf{p}_i in \mathcal{M} , and $\mathbf{A} = (A_1, \dots, A_{n_b})^t$ where A_i is an area weight of \mathbf{s}_i in $\partial\mathcal{M}$, so that for any Lipschitz function f on \mathcal{M} respectively $\partial\mathcal{M}$, $\int_{\mathcal{M}} f(\mathbf{x}) d\mathbf{x}$ respectively $\int_{\partial\mathcal{M}} f(\mathbf{x}) dS_x$ can be approximated by $\sum_{i=1}^n f(\mathbf{p}_i) V_i$ respectively $\sum_{i=1}^{n_b} f(\mathbf{s}_i) A_i$.

Based on above point cloud representation of the manifold, the integral equation (3.5) is discretized as

$$\begin{aligned} & \sum_{j=1}^n (1 - M(\mathbf{p}_i, \mathbf{p}_j)) R_t(\mathbf{p}_i, \mathbf{p}_j) (u_i - u_j) V_j + \sum_{j=1}^n \bar{R}_t(\mathbf{p}_i, \mathbf{p}_j) c(\mathbf{p}_j) u_j V_j \\ &= \sum_{j=1}^n \bar{R}_t(\mathbf{p}_i, \mathbf{s}_j) f(\mathbf{p}_j) V_j + 2 \sum_{\mathbf{s}_j \in S} \bar{R}_t(\mathbf{p}_i, \mathbf{s}_j) g(\mathbf{s}_j) A_j. \end{aligned} \quad (3.11)$$

Integral equation (3.7) and (3.10) also have corresponding discretization.

For the volume weights V and A in the discretization, we use methods in [25] to estimate them from the point cloud.

4 Numerical Examples

In this section, we will present numerical examples to demonstrate the performance of the point integral method for elliptic equation with variable coefficients. In the numerical examples, we solve the equation

$$D_i(a^{ij}(\mathbf{x})D_j u(\mathbf{x})) = f(\mathbf{x}) \quad (4.1)$$

with Neumann and Dirichlet boundary conditions.

The parameter t in the computations is chosen to be $t = \lambda_{\max}(\mathbf{A}(\mathbf{x}))\delta^2(\mathbf{x})$ where $\lambda_{\max}(\mathbf{A}(\mathbf{x}))$ is the largest eigenvalue of the matrix $\mathbf{A}(\mathbf{x}) = (a_{ij}(\mathbf{x})) = (a^{ij}(\mathbf{x}))^{-1}$ at $\mathbf{x} \in \mathcal{M}$, and $\delta(\mathbf{x})$ is the distance between \mathbf{x} and its 10th nearest neighbor. t is adaptive to the coefficients and the density of the sample points. It may be different at different point. Here we choose t such that there are enough points even in the direction with fastest changing (eigenvector of the coefficient matrix $\mathbf{A}(\mathbf{x})$ corresponding to the largest eigenvalue λ_{\max}). For Dirichlet boundary conditions, $\mu = 10^{-4}$ in (3.10).

4.1 Unit Disk and Annulus

In the first example, the computational domain \mathcal{M} is an unit disk in \mathbb{R}^2 . The exact solution is chosen to be $u_{gt} = x^2 - y^2$. In the second example, the exact solution is $u_{gt} = \sin(x+y)$ and the computational domain is an annulus in \mathbb{R}^2 with inner radius 1 and outer radius 3. The coefficient matrix (a^{ij}) is given in (4.2) in both of these two examples.

$$(a^{ij}(x,y)) = \frac{1}{r^4 + 2r^2 + 2} \begin{pmatrix} r^2 + 2 & -r \\ -r & r^2 + 1 \end{pmatrix}, \quad (4.2)$$

with $r = \sqrt{x^2 + y^2}$.

The errors in PIM are listed in Table 1. PIM converges in both of these two examples. The order of convergence is between 1 and 2 in both of these two examples.

PIM is also applicable in eigenvalue problem,

$$\sum_{i,j=1}^N D_i(a^{ij}(\mathbf{x})D_j u(\mathbf{x})) = \lambda u(\mathbf{x}) \quad (4.3)$$

For Neumann boundary, the integral equation is

$$\frac{1}{t} \int_{\mathcal{M}} (u(\mathbf{x}) - u(\mathbf{y})) (1 - M(\mathbf{x}, \mathbf{y})) R_t(\mathbf{x}, \mathbf{y}) d\mathbf{y} = \lambda \int_{\mathcal{M}} u(\mathbf{y}) \bar{R}_t(\mathbf{x}, \mathbf{y}) d\mathbf{y}, \quad (4.4)$$

Unit Disk				
$ V $	684	2610	10191	40296
Neumann	0.026258	0.016327	0.010253	0.006414
Dirichlet	0.033771	0.009291	0.002258	0.000923
Annulus				
$ V $	683	2624	10152	40578
Neumann	0.258189	0.100958	0.042372	0.017914
Dirichlet	0.044778	0.015825	0.004641	0.001614

Table 1: Errors in unit disk and annulus.

with

$$M(\mathbf{x}, \mathbf{y}) = -\frac{1}{2} \sum_{i,j,k=1}^N D_i a^{ij}(\mathbf{y}) a_{jk}(\mathbf{x}) (y^k - x^k). \quad (4.5)$$

For Dirichlet boundary, the integral approximation becomes

$$\begin{aligned} \frac{1}{t} \int_{\mathcal{M}} (u(\mathbf{x}) - u(\mathbf{y})) (1 - M(\mathbf{x}, \mathbf{y})) R_t(\mathbf{x}, \mathbf{y}) d\mathbf{y} + \frac{2}{\mu} \int_{\partial \mathcal{M}} u(\mathbf{y}) \bar{R}_t(\mathbf{x}, \mathbf{y}) d\tau_{\mathbf{y}} \\ = \lambda \int_{\mathcal{M}} u(\mathbf{y}) \bar{R}_t(\mathbf{x}, \mathbf{y}) d\mathbf{y}. \end{aligned} \quad (4.6)$$

with $\mu = 10^{-4}$ and $M(\mathbf{x}, \mathbf{y})$ is given in (4.5).

After discretization as described in Section 3.2, we get two generalized eigenvalue problem.

$$\sum_{j=1}^n (1 - M(\mathbf{p}_i, \mathbf{p}_j)) R_t(\mathbf{p}_i, \mathbf{p}_j) (u_i - u_j) V_j = \lambda \sum_{j=1}^n \bar{R}_t(\mathbf{p}_i, \mathbf{s}_j) u_j V_j, \quad (4.7)$$

and

$$\begin{aligned} \sum_{j=1}^n (1 - M(\mathbf{p}_i, \mathbf{p}_j)) R_t(\mathbf{p}_i, \mathbf{p}_j) (u_i - u_j) V_j + 2 \sum_{\mathbf{s}_j \in S} \bar{R}_t(\mathbf{p}_i, \mathbf{s}_j) u(\mathbf{s}_j) A_j \\ = \lambda \sum_{j=1}^n \bar{R}_t(\mathbf{p}_i, \mathbf{p}_j) u_j V_j. \end{aligned} \quad (4.8)$$

We solve the eigenvalue problems on an annulus with inner radius 1 and outer radius 3. The coefficient matrix (a^{ij}) is same as that in (4.2). We use the solutions given by finite element method with very fine mesh as the exact solution.

The first 20 eigenvalues are plotted in Figure 1. We can seen that the results of PIM converge to ground truth in both Neumann and Dirichlet problems. Eigenfunctions Dirichlet condition are shown in Figure 2.

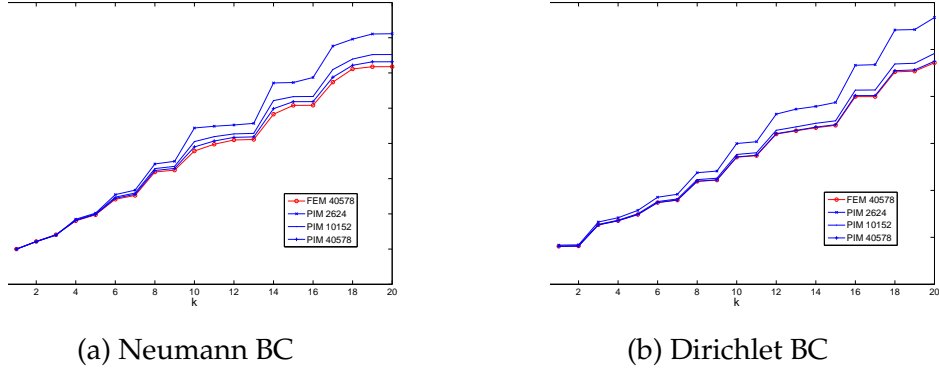


Figure 1: First 20 eigenvalues on the annulus. The numbers on the legends are numbers of sample points used in computation.

4.2 Spherical Cap

In this example, we consider a spherical cap in \mathbb{R}^3 . The height of the cap is $1/2$, thus the cap angle is $\pi/3$. We choose an orthonormal moving frame on the cap

$$e_1 = \frac{(-z, 0, x)}{\sqrt{1-y^2}}, \quad e_2 = \frac{(xy, y^2-1, yz)}{\sqrt{1-y^2}}.$$

The coefficient matrix is given by the a pullback metric in this moving frame. Let ϕ be the normal projection of the cap onto a disk in the $x-y$ plane. Pullback the standard Euclidean metric of the plane to the cap, we get

$$(a_{ij}) = \frac{1}{1-y^2} \begin{pmatrix} z^2 & -xyz \\ -xyz & x^2y^2 + (1-y^2)^2 \end{pmatrix}.$$

The coefficient matrix (a^{ij}) is the inverse of (a_{ij}) .

The exact solution is chosen to be the restriction of $u_{gt} = x+y+z$ on the cap. The errors of the numerical solutions are listed in Table 2. The convergence rates are approximately 1 and 2 for Neumann and Dirichlet problem respectively.

$ V $	1199	4689	18540	73757
Neumann	0.083855	0.045875	0.025878	0.013443
Dirichlet	0.020104	0.006967	0.001376	0.000456

Table 2: Solving for $u_{gt} = x+y+z$ on cap

The eigenvalue problems with Neumann and Dirichlet boundary conditions are also solved. The first 20 eigenvalues are plotted in Figure 3. And eigenfunctions are shown in Figure 4.

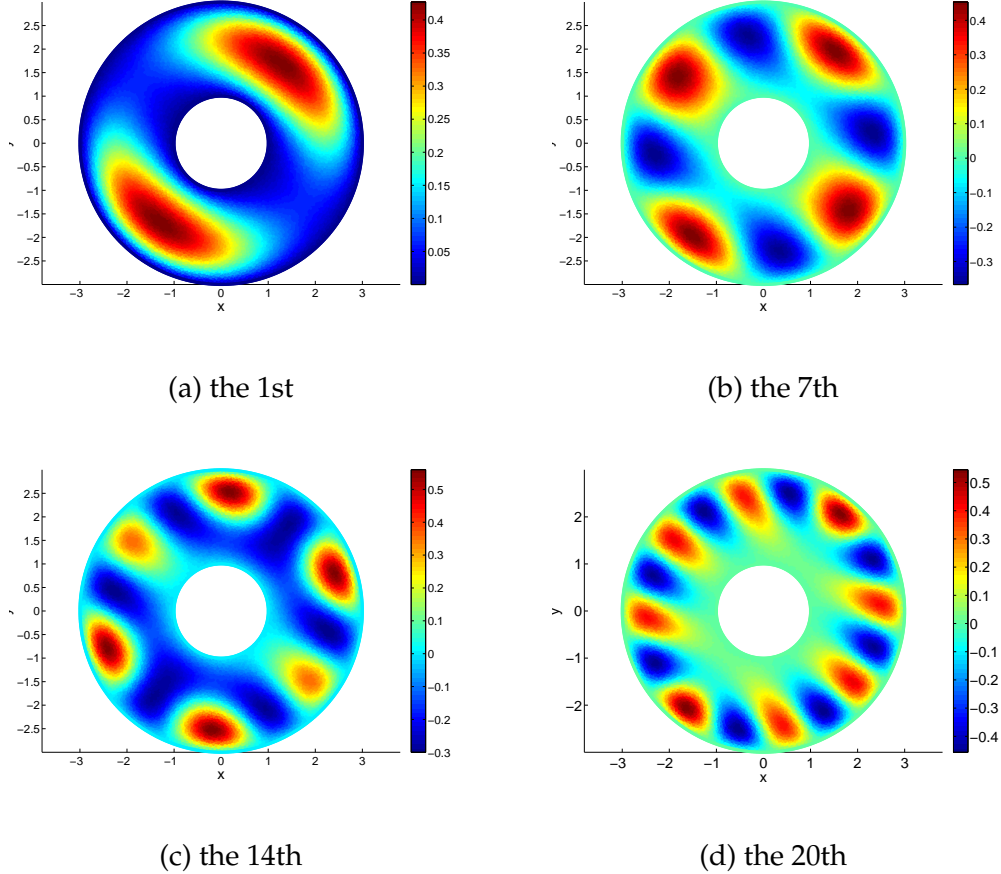


Figure 2: Examples of eigenfunctions on an annulus (Dirichlet BC).

4.3 Unit Sphere

Now, we consider the unit sphere S^2 in \mathbb{R}^3 . The unit sphere S^2 is sampled at random with uniform and non-uniform distribution. In the uniform sample, we first draw many points in \mathbb{R}^3 according to *isotropic* normal distribution:

$$\frac{1}{(2\pi)^{3/2}} \exp\left(-\frac{x^2+y^2+z^2}{2}\right). \quad (4.9)$$

And then project these points to unit sphere to get a uniform sample of S^2 .

In the non-uniform sample, the points in \mathbb{R}^3 are generated from an *anisotropic* normal distribution

$$\frac{1}{2(2\pi)^{3/2}} \exp\left(-\frac{x^2}{8}-\frac{y^2}{2}-\frac{z^2}{2}\right). \quad (4.10)$$

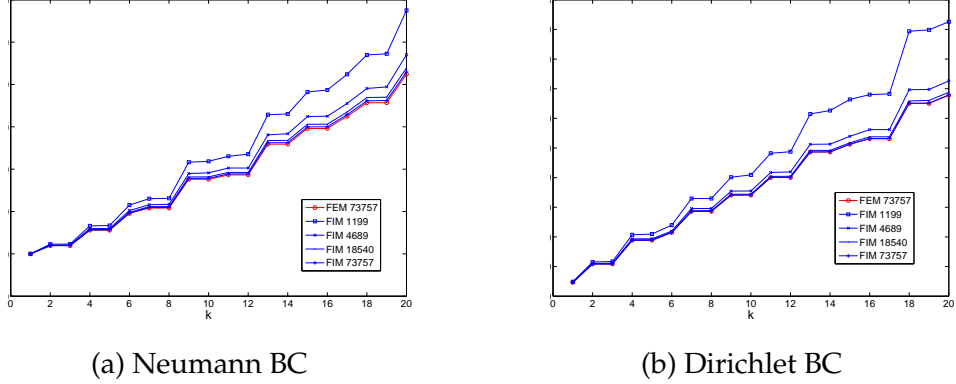


Figure 3: First 20 eigenvalues on the cap. The numbers on the legends are numbers of sample points used in computation.

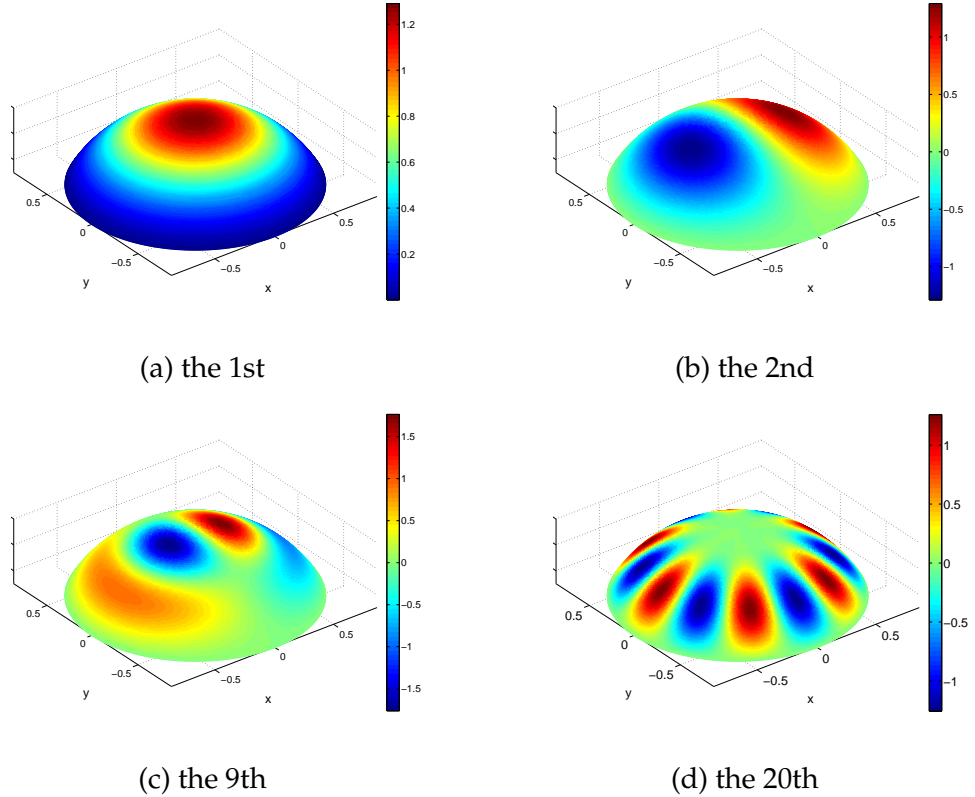


Figure 4: Examples of eigenfunctions on the cap (Dirichlet BC).

Then, the points are projected to unit sphere.

In uniform and non-uniform samples, we both draw 400, 1600, 6400 and 25600 points.

Figure 5 shows the uniform sampling and the non-uniform sampling with 6400 points

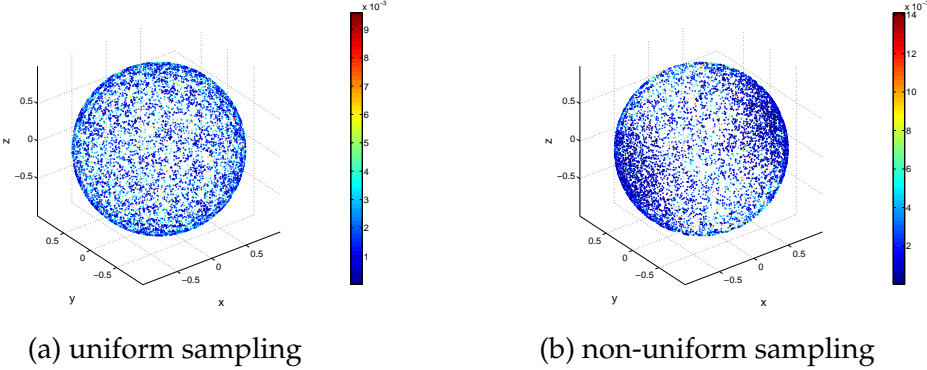


Figure 5: 6400 sample points on S^2 with volume weight in color.

In the test, the exact solution u_{gt} is the restriction of $x^2 - y^2 + z^2$ on S^2 . The relative L^2 errors are listed in Table 3 in different samples First, with uniform and non-uniform sample, PIM both converges. However, in uniform sample, the errors are lower than those in non-uniform samples.

N_P	400	1600	6400	25600
uniform	0.429105	0.279128	0.097547	0.071941
non-uniform	0.352364	0.202293	0.194980	0.123390

Table 3: L^2 error on S^2

4.4 Real Surfaces: Alex and Bunny

At the end of this section, we test PIM in two real surfaces: a human face called *Alex* and the surface of a rabbit called *Bunny*. "Alex" is a surface with boundary and "Bunny" is a closed surface. These two faces only have point cloud representation. "Alex" is sampled by 20953 points(Figure 6) and "Bunny" is sampled with 1227, 4904, 19611, 78440 points (Figure 7(a)).

on "Alex", the coefficient matrix is chosen to be

$$(a^{ij}) = \frac{1}{\sin(r/10)/2+1} \begin{pmatrix} 1 & 0 \\ 0 & 1 \end{pmatrix},$$

where $r = \sqrt{x^2 + y^2 + z^2}$.

With this isotropic coefficients, the eigenvalue problem is solved. Several eigenfunctions are shown in Figure 6.

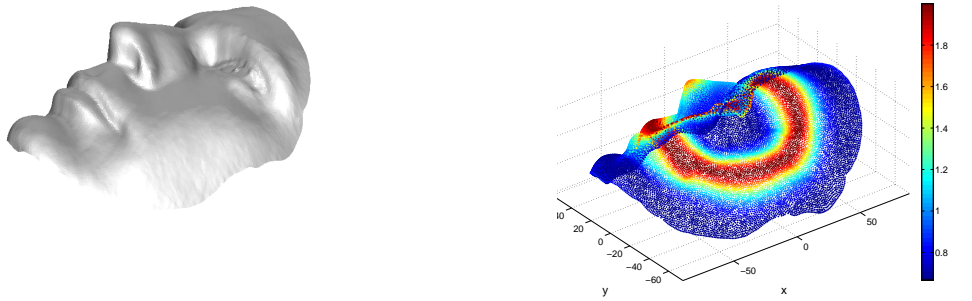
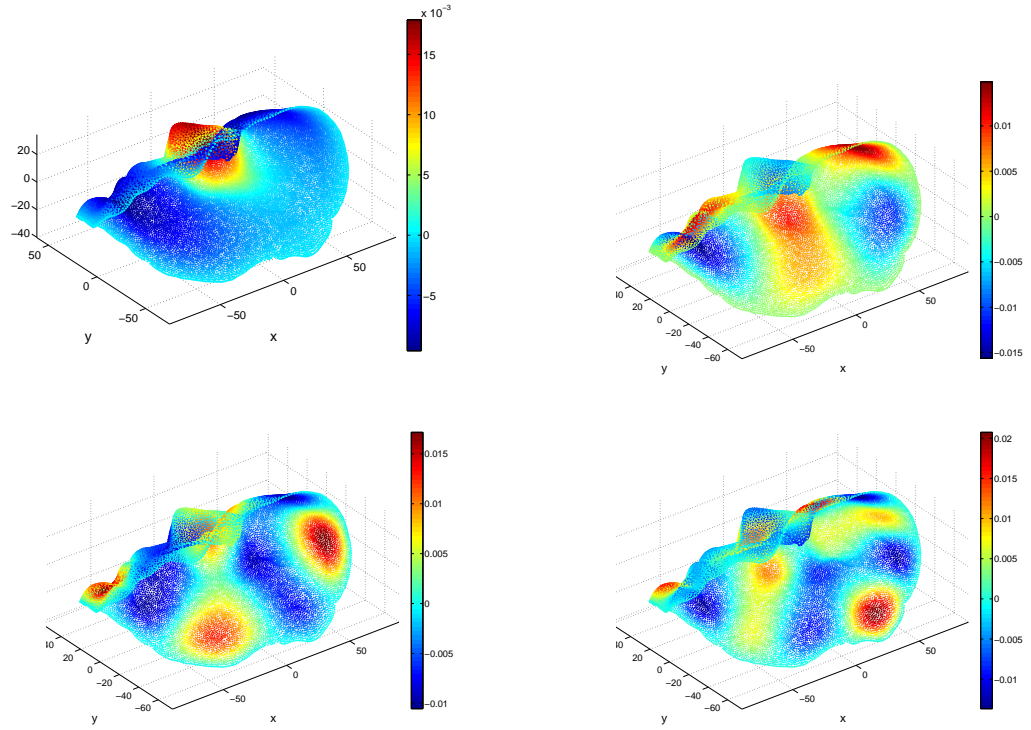
Surface \mathcal{M} : face of AlexCoefficient: restriction of $\frac{1}{\sin(R/10)/2+1}$ on \mathcal{M} 

Figure 6: Eigenfunctions on Alex's face

On the surface "Bunny", we solved the elliptic equation

$$-\sum_{i,j=1}^N (D_i a^{ij}(\mathbf{x}) D_j u(\mathbf{x})) = y$$

with

$$(a^{ij}) = \frac{1}{z^2+1} \begin{pmatrix} 1 & 0 \\ 0 & 1 \end{pmatrix},$$

where x, y, z are the Cartesian coordinates of the ambient space \mathbb{R}^3 . We use the homogeneous Dirichlet boundary condition. The computations are carried out in point clouds

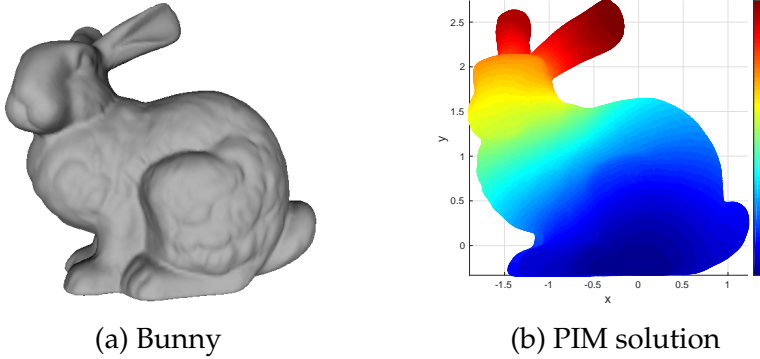


Figure 7: "Bunny" and one PIM solution.

with 1227, 4904, 19611, 78440 points. The PIM solution with 78440 points is shown in Figure 7(b).

We did the resolution study in the samples with 1227, 4904, 19611, 78440 points. To compute the differences of the solutions on different point clouds, we interpolate the solution between different point clouds. Fortunately, PIM gives a natural interpolation

$$I_{\mathbf{f}}(\mathbf{u})(\mathbf{x}) = \frac{\sum_{\mathbf{p}_j \in P} (1 - \frac{1}{2} M(\mathbf{x}, \mathbf{p}_j)) R_t(\mathbf{x}, \mathbf{p}_j) u_j V_j + t \sum_{\mathbf{p}_j \in P} \bar{R}_t(\mathbf{x}, \mathbf{p}_j) f_j V_j}{\sum_{\mathbf{p}_j \in P} (1 - \frac{1}{2} M(\mathbf{x}, \mathbf{p}_j)) R_t(\mathbf{x}, \mathbf{p}_j) V_j}. \quad (4.11)$$

The relative L^2 errors are listed in Table 4. The results suggest that the PIM in this example converges, however, the convergence rate is low.

Table 4: Solving elliptic equation on *Bunny*

$ V $	4904 v.s. 1227	19611 v.s. 4904	78440 v.s. 19611
error	0.718803	0.658242	0.574436

5 Conclusion

In this paper, we generalized the point integral method to solve the second order linear elliptic PDEs with smooth coefficients on point cloud. First, an integral equation is derived to approximate the original PDE. The main advantage of the integral equation is

that there is not any differential operators, thus easy to discretize over the point cloud. The local truncation error analysis shows that the L^2 error of the integral approximation is of order $t^{1/4}$, where t is a small parameter in the kernel function associate with the density of the points in the real computation. Then, the integral equation is discretized over the point cloud which gives a linear system. The numerical solution on the point cloud follows by solving this linear system.

The numerical experiments show that PIM is an effective method to solve the elliptic PDE on point cloud. There are still several drawbacks of the current version of the point integral method. The integral approximations in this paper do not preserve the symmetry of the original elliptic operator, which makes the convergence difficult to analyze. If the coefficients are isotropic, we can design another integral approximation which preserve the symmetry and the convergence has been also proved consequently [24]. Another drawback is that the convergence rate of PIM is low as shown in the numerical experiments. This is due to the low accuracy order in discretization of the integral equation. We are trying to use high order quadrature rule to discretize the integral equation to improve the accuracy of the point integral method.

A Approximation of Robin Boundary to Dirichlet Boundary

Theorem A.1. *If $u \in H^2(\mathcal{M})$ is the solution of the equation (1.5) with Dirichlet condition (3.8) and $u_\beta \in H^2(\mathcal{M})$ the solution of (1.5) with Robin condition (3.6), i.e.*

$$\begin{cases} -\sum_{i,j=1}^N D_i(a^{ij}(\mathbf{x})D_j u(\mathbf{x})) + \sum_{j=1}^N b^j(\mathbf{x})D_j u(\mathbf{x}) + c(\mathbf{x})u(\mathbf{x}) = f(\mathbf{x}), & \mathbf{x} \in \mathcal{M}, \\ u(\mathbf{x}) + \beta \sum_{i,j=1}^N n_i(\mathbf{x})a^{ij}(\mathbf{x})D_j u(\mathbf{x}) = g(\mathbf{x}), & \mathbf{x} \in \partial\mathcal{M}. \end{cases}$$

Let c_{min} be the minimum of c over \mathcal{M} , and $C(b) = \|b^j\|_\infty$. If the condition $4a_0c_{min} > C(a,b)^2$ holds where a_0 is the constant in the elliptic condition (1.6), then

$$\|u - u_\beta\|_{H^1(\mathcal{M})} \leq C\beta^{1/2}\|u\|_{H^2(\mathcal{M})}$$

Proof. Let $v = u - u_\beta$, then v is the solution of

$$\begin{cases} -\sum_{i,j=1}^N D_i(a^{ij}D_j v) + \sum_{j=1}^N b^j D_j v + cv = 0, & \mathbf{y} \in \mathcal{M}, \\ v + \beta \sum_{i,j=1}^N n_i a^{ij} D_j v = \beta \sum_{i,j=1}^N n_i a^{ij} D_j u, & \mathbf{y} \in \partial\mathcal{M}. \end{cases}$$

Multiply v on both sides of the above equation, integrate by parts, and use the boundary

condition for v and the properties of the coefficients, we get

$$\begin{aligned}
0 &= - \int_{\mathcal{M}} v \sum_{i,j=1}^N D_i(a^{ij} D_j v) \, d\mathbf{y} + \int_{\mathcal{M}} v \sum_{j=1}^N b^j D_j v \, d\mathbf{y} + \int_{\mathcal{M}} c v^2 \, d\mathbf{y} \\
&= \int_{\mathcal{M}} \sum_{i,j=1}^N a^{ij} D_i v D_j v \, d\mathbf{y} + \int_{\mathcal{M}} \sum_{j=1}^N b^j v D_j v \, d\mathbf{y} \\
&\quad - \int_{\partial\mathcal{M}} v \sum_{i,j=1}^N n_i a^{ij} D_j v \, d\tau_y + \int_{\mathcal{M}} c v^2 \, d\mathbf{y} \\
&\geq a_0 \int_{\mathcal{M}} |Dv|^2 \, d\mathbf{y} - C(a) \int_{\mathcal{M}} \sum_{i,j=1}^N |v| |D_j v| \, d\mathbf{y} \\
&\quad + \frac{1}{\beta} \int_{\partial\mathcal{M}} v^2 \, d\tau_y - \int_{\partial\mathcal{M}} v \sum_{i,j=1}^N n_i a^{ij} D_j u \, d\tau_y + \int_{\mathcal{M}} c v^2 \, d\mathbf{y},
\end{aligned}$$

where $C(b) = \|b^j\|_\infty$. By Cauchy-Schwartz inequality, we have

$$\begin{aligned}
\int_{\mathcal{M}} \sum_{i,j=1}^N |v| |D_j v| \, d\mathbf{y} &\leq \frac{1}{4\gamma} \int_{\mathcal{M}} v^2 \, d\mathbf{y} + \gamma \int_{\mathcal{M}} |Dv|^2 \, d\mathbf{y}, \\
\int_{\partial\mathcal{M}} v \sum_{i,j=1}^N n_i a^{ij} D_j u \, d\tau_y &\leq \frac{1}{4\beta} \int_{\partial\mathcal{M}} v^2 \, d\tau_y + \beta a_1 \int_{\partial\mathcal{M}} |Du|^2 \, d\tau_y,
\end{aligned}$$

where γ is any positive number. Therefore we have

$$C_1 \int_{\mathcal{M}} v^2 \, d\mathbf{y} + C_2 \int_{\mathcal{M}} |Dv|^2 \, d\mathbf{y} + \frac{3}{4\beta} \int_{\partial\mathcal{M}} v^2 \, d\tau_y \leq a_1 \beta \int_{\partial\mathcal{M}} |Du|^2 \, d\tau_y, \quad (\text{A.1})$$

where

$$C_1 = c_{min} - \frac{C(b)}{4\gamma}, \quad C_2 = a_0 - \gamma C(b),$$

and c_{min} is the minimum of c over \mathcal{M} . If the condition $4a_0c_{min} > C(b)^2$ holds, we can choose a γ such that $C_1 > 0$ and $C_2 > 0$. Then in the inequality (A.1), each term on the left side is no more than the right side. By trace theorem, there is

$$\int_{\partial\mathcal{M}} |Du|^2 \, d\tau_y \leq \|u\|_{H^2(\mathcal{M})}^2.$$

By Poincaré's inequality, we get

$$\|v\|_{H^1(\mathcal{M})}^2 \leq C\beta \|u\|_{H^2(\mathcal{M})}^2.$$

□

References

- [1] R. Barreira, C. Elliott, and A. Madzvamuse. Modelling and simulations of multi-component lipid membranes and open membranes via diffuse interface approaches. *J. Math. Biol.*, 56:347–371, 2008.
- [2] R. Barreira, C. Elliott, and A. Madzvamuse. The surface finite element method for pattern formation on evolving biological surfaces. *J. Math. Biol.*, 63:1095–1119, 2011.
- [3] M. Belkin and P. Niyogi. Laplacian eigenmaps for dimensionality reduction and data representation. *Neural Computation*, 15(6):1373–1396, 2003.
- [4] M. Bertalmio, L.-T. Cheng, S. Osher, and G. Sapiro. Variational problems and partial differential equations on implicit surfaces. *Journal of Computational Physics*, 174(2):759 – 780, 2001.
- [5] J. W. Cahn, P. Fife, and O. Penrose. A phase-field model for diffusion-induced grain-boundary motion. *Ann. Statist.*, 36(2):555–586, 2008.
- [6] P. T. Choi, K. T. Ho, and L. M. Lui. Spherical conformal parameterization of genus-0 point clouds for meshing. *SIAM Journal on Imaging Sciences*, 9(4):1582–1618, 2016.
- [7] P. T. Choi, K. C. Lam, and L. M. Lui. Flash: Fast landmark aligned spherical harmonic parameterization for genus-0 closed brain surfaces. *SIAM Journal on Imaging Sciences*, 8:67–94, 2015.
- [8] L. K. Chun and L. M. Lui. Landmark and intensity based registration with large deformations via quasi-conformal maps. *SIAM Journal on Imaging Sciences*, 7(4), 2014.
- [9] R. R. Coifman, S. Lafon, A. B. Lee, M. Maggioni, F. Warner, and S. Zucker. Geometric diffusions as a tool for harmonic analysis and structure definition of data: Diffusion maps. In *Proceedings of the National Academy of Sciences*, pages 7426–7431, 2005.
- [10] Q. Du, M. Gunzburger, R. B. Lehoucq, and K. Zhou. Analysis and approximation of nonlocal diffusion problems with volume constraints. *SIAM Review*, 54:667–696, 2012.
- [11] G. Dziuk. Finite elements for the beltrami operator on arbitrary surfaces. In S. Hildebrandt and R. Leis, editors, *Partial differential equations and calculus of variations*, volume 1357 of *Lecture Notes in Mathematics*, pages 142–155. Springer, 1988.
- [12] G. Dziuk and C. M. Elliott. Finite element methods for surface pdes. *Acta Numerica*, 22:289–396, 2013.
- [13] C. Eilks and C. M. Elliott. Numerical simulation of dealloying by surface dissolution via the evolving surface finite element method. *J. Comput. Phys.*, 227:9727–9741, 2008.
- [14] C. M. Elliott and B. Stinner. Modeling and computation of two phase geometric biomembranes using surface finite elements. *J. Comput. Phys.*, 229:6585–6612, 2010.
- [15] S. Ganesan and L. Tobiska. A coupled arbitrary lagrangian eulerian and lagrangian method for computation of free-surface flows with insoluble surfactants. *J. Comput. Phys.*, 228:2859–2873, 2009.
- [16] X. Gu, Y. Wang, T. F. Chan, P. M. Thompson, and S.-T. Yau. Genus zero surface conformal mapping and its application to brain surface mapping. *IEEE TMI*, 23:949–958, 2004.
- [17] A. J. James and J. Lowengrub. A surfactant-conserving volume-of-fluid method for interfacial flows with insoluble surfactant. *J. Comput. Phys.*, 201:685–722, 2004.
- [18] C.-Y. Kao, R. Lai, and B. Osting. Maximization of laplace-beltrami eigenvalues on closed riemannian surfaces. *ESAIM: Control, Optimisation and Calculus of Variations*, 23:685–720, 2017.
- [19] R. Lai, J. Liang, and H. Zhao. A local mesh method for solving pdes on point clouds. *Inverse Problem and Imaging*, 7:737–755, 2013.

- [20] R. Lai, Z. Wen, W. Yin, X. Gu, and L. Lui. Folding-free global conformal mapping for genus-0 surfaces by harmonic energy minimization. *Journal of Scientific Computing*, 58:705–725, 2014.
- [21] R. Lai and H. Zhao. Multi-scale non-rigid point cloud registration using robust sliced-wasserstein distance via laplace-beltrami eigenmap. *to appear in SIAM Journal on Imaging Sciences, arXiv:1406.3758.*, 2014.
- [22] S. Leung, J. Lowengrub, and H. Zhao. A grid based particle method for solving partial differential equations on evolving surfaces and modeling high order geometrical motion. *J. Comput. Phys.*, 230(7):2540–2561, 2011.
- [23] S. Leung and H. Zhao. A grid based particle method for moving interface problems. *J. Comput. Phys.*, 228(8):2993–3024, 2009.
- [24] Z. Li and Z. Shi. A convergent point integral method for isotropic elliptic equations on point cloud. *SIAM: Multiscale Modeling Simulation*, 14:874–905, 2016.
- [25] Z. Li, Z. Shi, and J. Sun. Point integral method for solving poisson-type equations on manifolds from point clouds with convergence guarantees. *Communications in Computational Physics*, 22(1):228–258, 2017.
- [26] J. Liang and H. Zhao. Solving partial differential equations on point clouds. *SIAM Journal of Scientific Computing*, 35:1461–1486, 2013.
- [27] L. M. Lui, X. Gu, T. F. Chan, and S. T. Yau. Variational method on riemann surfaces using conformal parameterization and its applications to image processing. *Methods & Applications of Analysis*, 15(4):513–538, 2008.
- [28] L. M. Lui, K. C. Lam, S. T. Yau, and X. Gu. Teichmuller mapping (t-map) and its applications to landmark matching registration. *SIAM Journal on Imaging Sciences*, 7(1):391–426, 2014.
- [29] L. M. Lui and C. Wen. Geometric registration of high-genus surfaces. *SIAM Journal on Imaging Sciences*, 7(1):337–365, 2013.
- [30] C. Macdonald and S. Ruuth. The implicit closest point method for the numerical solution of partial differential equations on surfaces. *SIAM J. Sci. Comput.*, 31(6):4330–4350, 2009.
- [31] T. W. Meng, P. T. Choi, and L. M. Lui. Tempo: Feature-endowed teichmller extremal mappings of point clouds. *SIAM Journal on Imaging Sciences*, 9(4):1922–1962, 2016.
- [32] T. W. Meng, P. T. Choi, and L. M. Lui. Tempo: Feature-endowed teichmller extremal mappings of point clouds. *SIAM Journal on Imaging Sciences*, 9:1582–1618, 2016.
- [33] M. P. Neilson, J. A. Mackenzie, S. D. Webb, and R. H. Insall. Modelling cell movement and chemotaxis using pseudopod-based feedback. *SIAM J. Sci. Comput.*, 33:1035–1057, 2011.
- [34] S. Osher, Z. Shi, and W. Zhu. Low dimensional manifold model for image processing. *accepted by SIAM Journal on Imaging Sciences*, 2017.
- [35] G. Peyré. Manifold models for signals and images. *Computer Vision and Image Understanding*, 113:248–260, 2009.
- [36] M. Reuter, F. E. Wolter, and N. Peinecke. Laplace-beltrami spectra as ‘shape-dna’ of surfaces and solids. *Computer Aided Design*, 38:342–366, 2006.
- [37] S. Ruuth and B. Merriman. A simple embedding method for solving partial differential equations on surfaces. *J. Comput. Phys.*, 227(3):1943–1961, 2008.
- [38] Z. Shi. Enforce the dirichlet boundary condition by volume constraint in point integral method. *Commun. Math. Sci.*, 15(6):1743–1769, 2017.
- [39] Z. Shi and J. Sun. Convergence of the point integral method for the poisson equation on point cloud. *Research in the Mathematical Sciences*, 4(1):22, 2017.
- [40] T. W. Wong, L. M. Lui, P. M. Thompson, and T. F. Chan. Intrinsic feature extraction on hippocampal surfaces and its applications. *SIAM Journal on Imaging Sciences*, 5(2):746–768, 2012.

- [41] J. Xu and H. Zhao. An eulerian formulation for solving partial differential equations along a moving interface. *J. Sci. Comput.*, 19:573–594, 2003.